Low-energy planar magnetic defects in $BaFe_2As_2$: Nanotwins, twins, antiphase, and domain boundaries

S. N. Khan,[1,2,*] Aftab Alam,[2,3,†] and Duane D. Johnson[1,2,4,‡]

[1]*Department of Physics, University of Illinois, Urbana-Champaign, Urbana, Illinois 61801, USA*

[2]*The Ames Laboratory, U.S. Department of Energy, Ames, Iowa 50011-3020, USA*

[3]*Department of Physics, Indian Institute of Technology, Mumbai 400 076, India*

[4]*Department of Materials Science & Engineering, Iowa State University, Ames, Iowa 50011-2300, USA*

(Received 20 April 2013; revised manuscript received 12 November 2013; published 27 November 2013)

In $BaFe_2As_2$, structural and magnetic planar defects begin to proliferate below the structural phase transition, affecting descriptions of magnetism and superconductivity. We study, using density-functional theory, the stability and magnetic properties of competing antiphase and domain boundaries, twins and isolated *nano*twins (twin nuclei), and spin excitations proposed and/or observed. These nanoscale defects have a very low surface energy (22–210 m Jm^{-2}), with twins favorable to the mesoscale. Defects exhibit smaller moments confined near their boundaries—making a uniform-moment picture inappropriate for long-range magnetic order in real samples. Nanotwins explain features in measured pair distribution functions so should be considered when analyzing scattering data. All these defects can be weakly mobile and/or can have fluctuations that lower assessed "ordered" moments from longer spatial and/or time averaging and should be considered directly.

DOI: 10.1103/PhysRevB.88.184515 PACS number(s): 74.20.−z, 74.25.Ha, 74.70.−b, 75.30.Kz

I. INTRODUCTION

Fe-based superconductors (FeSCs) provide another avenue to understanding unconventional superconductivity.[1–5] Due to its ease of synthesis, $BaFe_2As_2$ is a prototype for these systems, where its low-temperature ($T < 140$ K) ground state is a striped, antiferromagnetic (AFM) orthorhombic ($Fmmm$) structure,[6] often called a spin-density wave (SDW), which is reproduced in density-functional theory (DFT) calculations.[7] At the Neél temperature T_N (140 K), both a magnetic and a structural transition occur to a tetragonal ($I4/mmm$) paramagnet.[6] By doping with a transition metal at the Fe site or with others at Ba and As sites, superconductivity can be achieved, and similarly with pressure.[8–11]

There are strong connections between magnetism and superconductivity. Dopants weaken the magnetic state and Cooper pairing is, perhaps, driven by increased magnetic fluctuations out of the ground state.[12,13] DFT has proven successful in modeling the geometry, magnetic ordering, and electronic structure of FeSCs. The magnetic ground states of LaFeAsO, $BaFe_2As_2$, NaFeAs, and FeTe were all correctly predicted.[7,14–16] Fermi-surface (FS) nesting is apparent from DFT calculations and agrees with angle-resolved photoemission spectroscopy, suggesting an itinerant nature,[17–19] which is supported by the spin-wave dispersion.[20,21] Furthermore, DFT explains quantitatively the effects of doping on FS nesting and why Cu doping behaves differently than Co and Ni doping.[22] $K_xFe_2Se_2$ (isostructural to $BaFe_2As_2$) does not have the hole pockets needed for FS nesting,[23] as DFT reveals.[24]

DFT results for $BaFe_2As_2$ show a strong coupling between structure and magnetism.[17,25] Planar defects, thus, have been proposed to explain key features in the magnetic and transport properties of FeSCs near/below the structural transition. Mazin and Johannes[26] suggested a model in which low-energy magnetic antiphase boundaries (APBs) and 90° domain boundaries (DBs) proliferate (Fig. 1), which have yet to be tested. So, are structural and magnetic planar defects energetically favorable, and what are their properties? To answer these questions, we use DFT to model potentially operative magnetic (structural-induced) defects, both isolated and extended, and explore their stability and properties by varying the structural parameters.

II. BACKGROUND

Defects can be very important in realistic materials, like $BaFe_2As_2$. Above T_N, the paramagnetic state may be realized by mobile APBs and DBs; below T_N, with interlayer coherence, APBs become pinned and DBs thermodynamically inaccessible, possibly explaining the sensitivity to interlayer elements, high magnetoresistance, features of the differential resistivity ($d\rho/dT$), and invariance of resistivity anisotropy. With orthorhombic distortions ($a > b$), both structural and concomitant magnetic twins (Fig. 2) are observed in $BaFe_2As_2$ along $\langle 110\rangle$ with 100–400 nm[27] up to 10–50 μm[28] between boundaries. With stress, samples detwin, but twins return upon its removal;[29] as in $YBa_2Cu_3O_{7-\delta}$,[30] $(1\bar{1}0)$ twins terminate on (110) twins. Twins cause anisotropic scattering near AFM wave vectors, giving two-dimensional spin fluctuations. Twins also create stripes of increased diamagnetic response[31] and nucleate superconductivity at their boundaries.[32] Recently, Niedziela *et al.*[33] found, by Rietveld analysis, a higher orthorhombic ratio [$O = (a - b)/(a + b)$] for local structural fits ($O = 1.38\%$) than for global fits ($O = 0.78\%$); they proposed that a high density of *nano*twins (Fig. 2) accounts for this discrepancy by its better match to measured pair distribution functions. We show that displacements at the *nano*twin boundary affect the spin alignment, reducing the average "ordered" moment.

For completeness, we note that, while DFT supports the observed SDW for the parent compound, the Fe moment ($1.6–1.9\mu_B$)[7,34] is twice that assessed for the average ordered moment from neutron diffraction ($0.8–1.04\mu_B$).[35–37] In fact, various experiments assess very different Fe moments. Core-electron spectroscopy[38] finds $2.1\mu_B$, like DFT, while ^{57}Fe

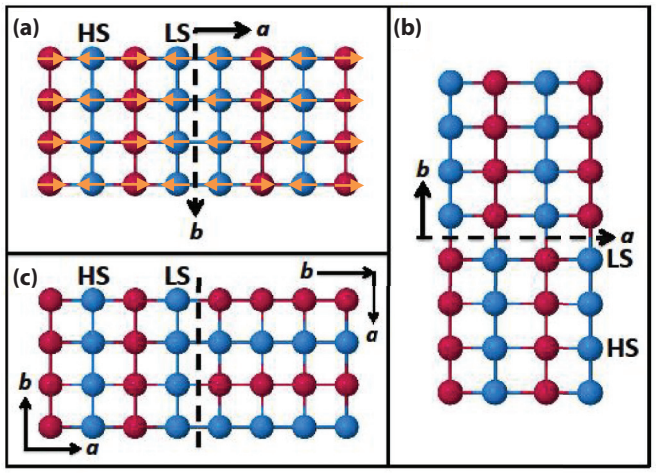

FIG. 1. (Color online) (a) APB in the bc plane, (b) APB in the ac plane, and (c) 90° DB with no strain ($a = b$). Red (blue) circles are "up" ("down") in-plane moments, as indicated in (a). HS, MS, and LS indicate Fe sites with high-, medium-, and low-spin states.

Mössbauer[6] and nuclear magnetic resonance[39] find $0.81\mu_B$, as in diffraction assessments. For Fe-based magnets such a large discrepancy between ordered moments from theory and experiment is unusual. Spin-orbit and hybridization (controlled by Fe/As planar spacing) in a DFT + U model explained the small in-plane moments in Fe-pnictides.[40] Yet our DFT moments are reduced by ∼10% by spin-orbit, but by 50%–100% by slightly reduced Fe-As spacing. DFT predicts correct moments at the short times (∼10^{-15} s) necessary to yield lattice constants that agree with experiment.[26] Dynamical mean-field theory explains the discrepancy from DFT as a result of dynamical fluctuations at the Fe sites that reduce the observed moment over longer time scales (∼10^{-9} s)[41] and reproduces the trends in reduced Fe moments and renormalized mass across various FeSCs.[42] Dynamical mean-field theory finds that FeSCs are correlated due to intra-atomic exchange from Hund's coupling J (0.3–0.6 eV)[43–46] (which reduces the coherence temperature for Fermi liquid behavior),[45] not from especially large U (2.8–5.2 eV, as derived from a five-band constrained random phase approximation)[44,46–48] or proximity to a Mott insulating state. Below the coherence temperature,

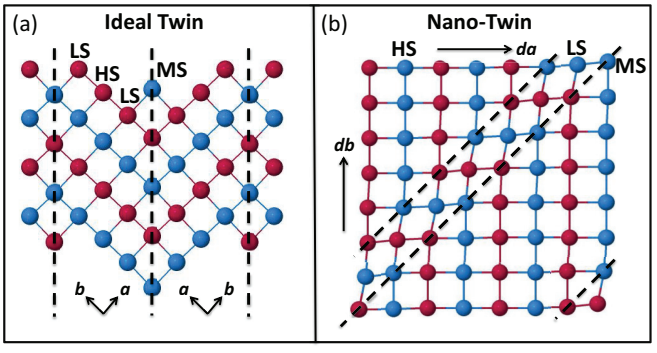

FIG. 2. (Color online) (a) Twin boundary, without strain, separated by three Fe layers. (b) Nanotwin with boundary ⊥ to (110), where atom positions in a distorted cell are barycentric weights of the cell corners. HS, MS, and LS states are indicated.

a high electron mobility results in moment screening (over 10^{-9} s). Notably, this scenario does not consider spatial fluctuations, defects, or their effect on magnetism near/below the phase transition, as explored in the present work.

III. METHODS: DEFECTS AND DFT

We use DFT to simulate various magnetic planar defects, i.e., two types of APBs, a 90° DB, twin boundaries, and our modified *nano*twin, which are all low-energy excitations of the SDW. Figures 1(a) and 1(b) show two APB boundaries in the Fe-plane—parallel to the bc or ac planes—and Fig. 1(c) shows a locally unstrained 90° DB. Figure 2(a) shows a typical example of an ideal twin. A modified nanotwin with two-dimensional structural distortion (consistent with that suggested by Niedziela *et al.*)[33] is shown in Fig. 2(b) with a series of static displacements along the a and b axes in the supercell. The undisplaced nanotwin with one layer of Fe separating defect planes is really a magnetic stacking fault; a nanotwin supercell has very different boundary conditions than a twin does, with different far neighbors and distances between defect pairs; indeed, an "ideal-twin" supercell formed with one-layer separation between defect planes (a high density of stacking faults) has local environments like the nanotwin's, except that the twin has symmetric relaxations governed by the supercell periodicity, whereas the nanotwin has asymmetric, localized distortions to match the pair distribution function. While we show that the defect energies are similar, a nanotwin, due to its boundary condition and supercell, may be considered a fluctuating twin nuclei, which can have low-spin (LS) Fe sites unavailable in the ideal-twin supercell.

For nondefected (parent) and defected cells we calculate the energy per atom and the associated magnetic moments (the bulk is $1.6\mu_B$). From this we derive the planar defect energy, γ, defined as $\gamma = (E_{\rm def} - E_0)d/V$, where $E_{\rm def}$ and E_0 are the total *energy per atom* of the defected and nondefected cells, respectively. d is the distance between defect planes and V is the volume per atom. While the energy per atom is helpful, γ is the appropriate comparison for the cost of creating the defect interface and its dependence on the defect density and defect volume. Note that two defect boundaries are created for twins, hence, 2γ is the appropriate defect energy.

To do this, we use VASP[49] with the plane-wave pseudopotential projected augmented wave (PAW) basis,[50] with an energy cutoff of 380–420 eV. A Monkhorst-pack Brillouin-zone integration with a 16^3 **k** mesh is used for the SDW ($Fmmm$) structure. Smaller **k** meshes are used for supercells, depending on the length coverage along each axis.

For APBs, we constructed doubled ($2 \times 1 \times 1$), quadrupled, and octupled supercells to examine excitations, denoted 2-APB, 4-APB, and 8-APB, respectively (Fig. 3). For APBs [Figs. 1(a) and 1(b)], we use measured lattice parameters[6] ($a = 5.6146$ Å, $b = 5.5742$ Å, and $c = 12.9453$ Å). For the 90° DB, we set $\bar{a} = \bar{b} = (a + b)/2 = 5.5944$ Å to reduce local strain effects and construct supercells similar to the APBs, denoted 2-DB, 4-DB, and 8-DB. Twin $[4(1 + n) \times 2 \times 1]$ supercells ($n = 0, 1, \ldots$) are denoted by $(3 + 4n)$-N Fe layers between defect planes and have $4(1 + n)$ unit cells along a and $8(1 + n) \times 10$ atoms/cell. Nanotwin supercells are denoted 3-N, 5-N, 9-N, and 13-N for Fe layers between isolated

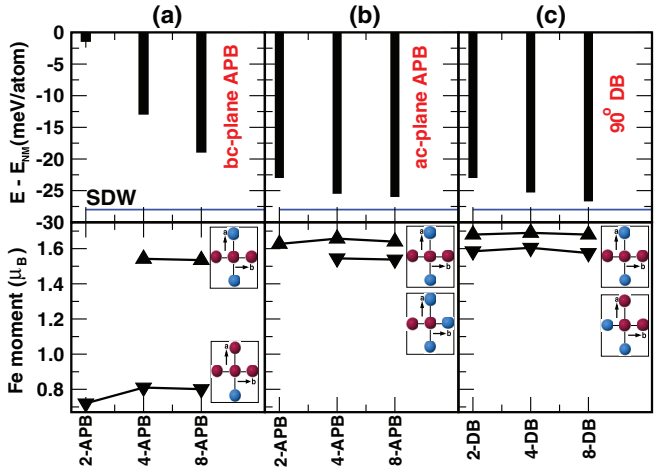

FIG. 3. (Color online) Energies relative to the nonmagnetic state (top) and Fe moments (bottom) for (a) APBs in the *bc* plane (b) APBs in the *ac* plane, and (c) 90° DB. SDW indicates the AFM ground state. Insets: Local Fe environment.

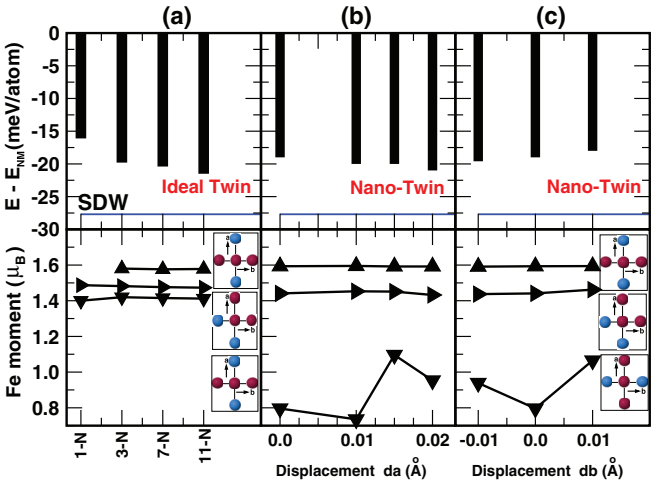

FIG. 4. (Color online) Same as Fig. 3, but for (a) twins (labels defined in text) and for nanotwins ($3 \times 3 \times 2$ supercell) with displacements (a) along the *da* axis and (c) along the *db* axis. Insets: Fe has HS, MS, and LS states due to the local environment.

nanotwin pairs; the supercells with the static displacements suggested by Niedziela *et al.* are more complex because the local distortions must be compensated within the cell [Fig. 2(b)].

IV. RESULTS

The energies and moments for APB and DB defects relative to the nonmagnetic state are shown in Fig. 3 (top) and compared to the AFM ground state (SDW). In all cases, Fe moments have two behaviors: a high-spin (HS) state (see Fig. 1) at sites away from boundaries and an LS state (see Fig. 1) at/near boundaries. For the APB(bc), the LS moment falls substantially, from $1.6\mu_B$ to $0.8\mu_B$, similarly to that found by Yin *et al.*[51] However, for the APB(ac), the LS moment decreases only to $1.54\mu_B$. The two spin states depend on the local magnetic environments (Fig. 3 inset). Moments do not vary much with the size of the supercells, but these two structures energetically compete with the ground-state SDW ($\leqslant$9 meV/atom). For the 90° DB [Fig. 1(c)], the HS state has the higher moment of $1.7\mu_B$ due to global strain from the changed lattice parameters. The LS moment decreases slightly, to $1.57\mu_B$, near the boundary. Formation of this defect requires within 2 meV/atom excess energy compared to the SDW. It energetically competes with the APB(ac). Both defects are then expected to be present at the same temperature. The local environment does not play a significant role, suggesting that simple models such as counting the number of aligned neighbors are not sufficient to characterize the moments.

The energy and moments for twins are shown in Fig. 4(a). Interestingly, an Fe atom in a twin has three spin states, depending on the local environment. Fe atoms at the boundary remain in a medium-spin (MS) state [see Fig. 2(a)]. An LS state occurs at Fe sites adjacent to the boundary [Fig. 2(a)]. These Fe sites have the same nearest-neighbor environment as the bulk HS states but differ in the farther neighbors. These defects can form at a few milli–electron volts per atom, albeit γ is more critical (see below).

Nanotwin energies and moments versus distortion along the a and b axes (in Å) are shown in Figs. 4(b) and 4(c). Similarly to twins, there are three Fe spin states: an HS bulk ($1.6\mu_B$), an MS at the boundary ($1.42\mu_B$), and an LS in the vicinity of the distorted side of the boundary (0.8–$1.0\mu_B$). The structural perturbations show a stronger effect on the LS moments near defect boundaries, decreasing to as low as $0.8\mu_B$. Isolated (fluctuating) nanotwins are equally competitive to form as dense twins, but with much reduced moments. Energies are affected mostly by the changed magnetic configurations and very little by spatial distortions. So magnetic defects drive the short-range structural distortion (not the other way around) and can help quench magnetization.

Planar defect energies (γ or $2\gamma_{\text{twins}}$) are compared in Table I; they give the relative order in which magnetic defects can form and remain after processing. Structural defects can act as pinning sites for magnetic domain walls. Energetically, the APB(ac), the 90° DB, and nanotwins (low-energy spin excitations) are the most favorable and the most likely to persist after annealing. Interestingly, densely packed twins of a single tetragonal variant also have a very low energy. These nanoscale defects compete with widely separated twins (spin kinks), which are observed. Such small fluctuating defects will affect the observed average moments, whereas separated twins will affect the magnetic correlation length(see below). Separated twins do form and are stabilized by lattice strain arising from disclinations formed when twins oriented 90° apart (from the two tetragonal variants) intersect.[30] It is the twin-twin interactions that stabilize the mesoscale twins.

Typically in metals, the calculated $2\gamma_{\text{twin}}$ is monotonically decreasing versus d (the separation of the twin boundaries) until it plateaus at the measured twin boundary energy; essentially, the defects interact (costing energy) until separated enough that they are screened from one another. Strikingly, in $BaFe_2As_2$, separated twins are higher in energy than dense twins, until a d of 16 unit cells (15 Fe layers), where $2\gamma_{\text{twin}}$ reaches a maximum (Table I and Fig. 5), after which there

TABLE I. γ (2γ for twins) for various planar defects (in mJ/m^2). Energies (in meV/atom) are relative to the SDW. γ_{twin} is dominated by d's increasing more rapidly than the decrease in $(E_{\text{def}} - E_0)$, unlike for APBs or DBs.

Defect type	Supercell	Energy	γ (2γ)
APB (*bc* plane)	2-APB	26.5	118
	4-APB	15.0	133
	8-APB	9.0	160
APB (*ac* plane)	2-APB	5.0	22
	4-APB	2.5	22
	8-APB	2.0	35
90° DB	2-DB	5.0	22
	4-DB	2.7	24
	8-DB	1.3	22
"Twin" (ideal)	0-N	18.3	57
"Twin" (relaxed)	1-N	9.9	62
"Twin" (ideal)	1-N	11.9	74
Twin (ideal)	3-N	8.2	102
	7-N	6.6	165
	11-N	6.1	228
	15-N	5.0	(max) 252
	19-N	3.7	231
	23-N	3.0	222
	27-N	2.4	210
Nanotwin (undistorted)	3-N	9.2	86
	5-N	6.4	80
	9-N	4.1	77
	13-N	2.5	63
Nonmagnetic bulk	10 atoms	28.0	n/a

is a slow convergence of $2\gamma_{\text{twin}}$ versus d (Fig. 5). At 28 unit cells (~11 nm), $2\gamma_{\text{twin}}$ has not yet converged, emphasizing the long-range interactions among twins. Observed structural twins[27,28] are extended well beyond those computationally feasible. Thus, higher-density twins should become prominent near the phase transition, where they compete with the ground state.

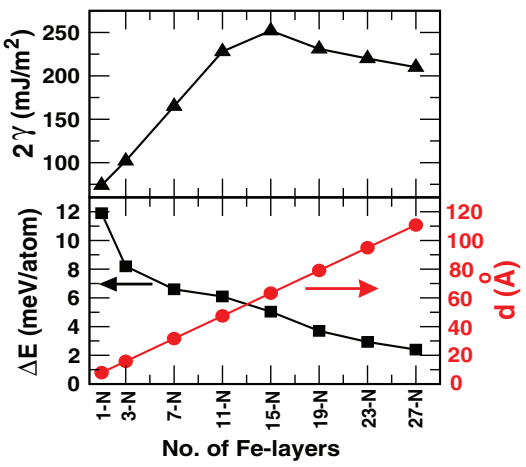

FIG. 5. (Color online) Twin energy 2γ (top) and $\Delta E = (E_{\text{def}} - E_0)$ and d (bottom) versus number of Fe layers.

V. DISCUSSION

Twin separation d is also affected by stress. Equilibrium is typically reached when the applied stress is $\sim 2\gamma_{\text{twin}} d$, which is, however, exceedingly low for isolated twins in $BaFe_2As_2$. In real samples twins appear in 90°-oriented pairs, where $(1\bar{1}0)$ twins terminate on (110) twins; this configuration is stabilized by lattice strain arising from disclinations,[30] where the strain is reduced at the cost of an increased d. With stress (estimated roughly from a set of disclinations[30] and orders of magnitude larger than $2\gamma_{\text{twin}} d$), samples detwin, but twins will (and do) return upon its removal.[29]

Twins cause anisotropic scattering near AFM wave vectors, giving two-dimensional spin fluctuations, and create stripes of increased diamagnetic response.[31] While twin separation depends on local defects and stress, it is expected to cause a peak in the magnetic susceptibility $\chi(q)$ at $q = 2\pi/\hat{d}$, where $\hat{d}$ is the average twin-twin separation at which 2γ saturates. The direction of q is perpendicular to the twin boundaries [i.e., 45° to reciprocal-space k_x and k_y axes, where x (y) is along the a (b) axis]. While the twins dictate the magnetic correlation length, we suggest that small, low-energy excitation can further depress average moments by spatial and temporal averaging, beyond that due to dynamic fluctuations.

Nanotwins [Fig. 2(b)] with no local distortion are like an isolated, ideal defect pair, not a dense set of twins. To understand the effect of short-ranged structural distortion, we have studied a 1-N ideal twin with (and without) relaxation in the ab plane for only those atoms near the boundary, more localized than in the nanotwin supercell. The planar defect energy with (without) relaxation is 62 (74) mJ/m^2. Relaxations along the a and b axis lie within 0.9% of ideal, close to the best fit to measured pair distribution functions,[33] so the twin and nanotwin are very similar in energy and local structure. Unlike for ideal twins, the nanotwin surface energy decreases to its limiting value as the nanotwin-nanotwin distance grows (Table I), and it is much lower than that for extended twins. Thus, a nanotwin may be considered a fluctuating twin nucleus, which has many more LS sites (Fig. 4) not available in a twin supercell, with moments as low as $0.8\mu_B$ near the defect, similarly to the assessed values in $BaFe_2As_2$. Our calculations support Niedziela *et al.*'s suggestion[33] that nanotwins constitute an important fluctuating excitation in $BaFe_2As_2$.

Because the local magnetic configurations play the key role in determining the spin states of Fe, we calculated the site- and l-projected density of states (DOS) to understand the electronic-structure origin. Figure 6 shows the Fe d-projected DOS for HS and LS states. For the bulk (HS) states, the major contribution at the Fermi energy E_F arises from Fe d_{xz} and $d_{3z^2-r^2}$, also evidenced by angle-resolved photoemission spectroscopy.[52] All the other orbital components exhibit a pseudogap near E_F. For LS Fe compared to HS Fe, all the projected DOS values are shifted towards E_F. The most pronounced effect occurs for d_{xz} and $d_{3z^2-r^2}$ character, where the majority states for LS fall into a pseudogap for d_{xz} but are peaked for $d_{3z^2-r^2}$. Although the change in these orbital states is dominated by in-plane Fe spin configurations, small contributions also arise from the hybridization with As p_x and

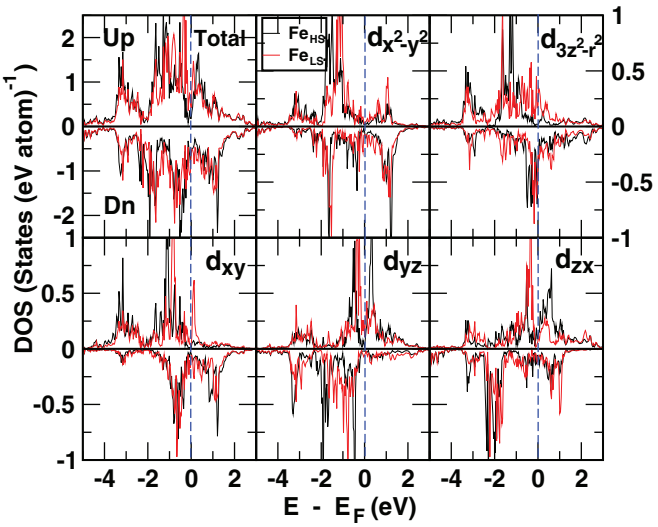

FIG. 6. (Color online) The d-orbital and spin-projected DOS of an undistorted nanotwin at HS (black line) and LS [lighter (red) line] Fe sites, with the majority (minority) DOS plotted on the positive (negative) vertical axis. The Fermi energy is indicated by the dashed vertical (blue) line. The x, y, and z directions correspond to a, b, and c, respectively.

p_y orbitals (out of the Fe plane), eventually altering the FS. The large difference in the near-E_F (majority) DOS between the HS and the LS states points to an orbital-dependent electronic origin for quenched moments.

VI. SUMMARY

In summary, we have studied competing low-energy, magnetic planar defects in $BaFe_2As_2$. The favorable defects are the APB(ac), the 90° DB, and nanotwins, but twins (which are observed) are favorable through the mesoscale. The most pronounced reductions in Fe moment are near the boundaries of APBs(bc) and nanotwins. We find that isolated, closely spaced twins (twin nuclei) are energetically favorable and correspond to a recently proposed nanotwin suggested to match the pair distribution function from scattering experiments.[33] Nanotwins are energetically insensitive to microscopic displacements near the boundary, in contrast to their sensitivity to the As z coordinate. APBs along bc planes and ac planes are not equally favorable, an anisotropy not anticipated in the Mazin and Johannes model.[26] These defects can reduce the Fe moment from spatial averaging, an environmental dependence which is not included in dynamical mean-field theory.[41,42] Assessing these defects and their dynamics can affect the magnetism, which can be evaluated via Monte Carlo simulations and these future studies are planned.

ACKNOWLEDGMENTS

This work was supported by the US Department of Energy (DOE), Office of Basic Energy Science, Division of Materials Science and Engineering (seed funding), and, for S.N.K., by the Center for Defect Physics, an Energy Frontier Research Center at ORNL. The Ames Laboratory is operated for the US DOE by Iowa State University under Contract No. DE-AC02-07CH11358.

*snkhan@illinois.edu
†aftab@phy.iitb.ac.in
‡ddj@ameslab.gov

[1] G. R. Stewart, Rev. Mod. Phys. **83**, 1589 (2011).
[2] H.-H. Wen and S. Li, Annu. Rev. Condens. Matter Phys. **2**, 121 (2011).
[3] P. C. Canfield and S. L. Bud'ko, Ann. Rev. Condens. Matter Phys. **1**, 27 (2010).
[4] J. Paglione and R. L. Greene, Nat. Phys. **6**, 645 (2010).
[5] A. A. Kordyuk, Low Temp. Phys. **38**, 888 (2012).
[6] M. Rotter, M. Tegel, D. Johrendt, I. Schellenberg, W. Hermes, and R. Pöttgen, Phys. Rev. B **78**, 020503 (2008).
[7] D. J. Singh, Phys. Rev. B **78**, 094511 (2008).
[8] N. Ni, M. E. Tillman, J.-Q. Yan, A. Kracher, S. T. Hannahs, S. L. Bud'ko, and P. C. Canfield, Phys. Rev. B **78**, 214515 (2008).
[9] N. Ni, A. Thaler, J. Q. Yan, A. Kracher, E. Colombier, S. L. Bud'ko, P. C. Canfield, and S. T. Hannahs, Phys. Rev. B **82**, 024519 (2010).
[10] P. L. Alireza, Y. T. C. Ko, J. Gillett, C. M. Petrone, J. M. Cole, G. G. Lonzarich, and S. E. Sebastian, J. Phys.: Condens. Matter **21**, 012208 (2009).
[11] M. S. Torikachvili, S. L. Bud'ko, N. Ni, and P. C. Canfield, Phys. Rev. B **78**, 104527 (2008).
[12] K. Kuroki, S. Onari, R. Arita, H. Usui, Y. Tanaka, H. Kontani, and H. Aoki, Phys. Rev. Lett. **101**, 087004 (2008).
[13] F. Wang, H. Zhai, Y. Ran, A. Vishwanath, and D.-H. Lee, Phys. Rev. Lett. **102**, 047005 (2009).
[14] I. I. Mazin, M. D. Johannes, L. Boeri, K. Koepernik, and D. J. Singh, Phys. Rev. B **78**, 085104 (2008).
[15] S. Li, C. de la Cruz, Q. Huang, G. F. Chen, T.-L. Xia, J. L. Luo, N. L. Wang, and P. Dai, Phys. Rev. B **80**, 020504 (2009).
[16] F. Ma, W. Ji, J. Hu, Z.-Y. Lu, and T. Xiang, Phys. Rev. Lett. **102**, 177003 (2009).
[17] D. J. Singh and M.-H. Du, Phys. Rev. Lett. **100**, 237003 (2008).
[18] S. Ideta, T. Yoshida, I. Nishi, A. Fujimori, Y. Kotani, K. Ono, Y. Nakashima, S. Yamaichi, T. Sasagawa, M. Nakajima, K. Kihou, Y. Tomioka, C. H. Lee, A. Iyo, H. Eisaki, T. Ito, S. Uchida, and R. Arita, Phys. Rev. Lett. **110**, 107007 (2013).
[19] P. Richard, K. Nakayama, T. Sato, M. Neupane, Y.-M. Xu, J. H. Bowen, G. F. Chen, J. L. Luo, N. L. Wang, X. Dai, Z. Fang, H. Ding, and T. Takahashi, Phys. Rev. Lett. **104**, 137001 (2010).
[20] L. W. Harriger, H. Q. Luo, M. S. Liu, C. Frost, J. P. Hu, M. R. Norman, and P. Dai, Phys. Rev. B **84**, 054544 (2011).
[21] R. A. Ewings, T. G. Perring, R. I. Bewley, T. Guidi, M. J. Pitcher, D. R. Parker, S. J. Clarke, and A. T. Boothroyd, Phys. Rev. B **78**, 220501 (2008).
[22] M. G. Kim, J. Lamsal, T. W. Heitmann, G. S. Tucker, D. K. Pratt, S. N. Khan, Y. B. Lee, A. Alam, A. Thaler, N. Ni, S. Ran, S. L. Bud'ko, K. J. Marty, M. D. Lumsden, P. C. Canfield, B. N. Harmon, D. D. Johnson, A. Kreyssig, R. J. McQueeney, and A. I. Goldman, Phys. Rev. Lett. **109**, 167003 (2012).
[23] J. Guo, S. Jin, G. Wang, S. Wang, K. Zhu, T. Zhou, M. He, and X. Chen, Phys. Rev. B **82**, 180520 (2010).

[24]C. Cao and J.-H. Dai, Chin. Phys. Lett. **28**, 057402 (2011).
[25]E. Aktürk and S. Ciraci, Phys. Rev. B **79**, 184523 (2009).
[26]I. I. Mazin and M. D. Johannes, Nat. Phys. **5**, 141 (2009).
[27]C. Ma, H. X. Yang, H. F. Tian, H. L. Shi, J. B. Lu, Z. W. Wang, L. J. Zeng, G. F. Chen, N. L. Wang, and J. Q. Li, Phys. Rev. B **79**, 060506 (2009).
[28]M. A. Tanatar, A. Kreyssig, S. Nandi, N. Ni, S. L. Bud'ko, P. C. Canfield, A. I. Goldman, and R. Prozorov, Phys. Rev. B **79**, 180508 (2009).
[29]M. A. Tanatar, E. C. Blomberg, A. Kreyssig, M. G. Kim, N. Ni, A. Thaler, S. L. Bud'ko, P. C. Canfield, A. I. Goldman, I. I. Mazin, and R. Prozorov, Phys. Rev. B **81**, 184508 (2010).
[30]A. H. King and Y. Zhu, Philos. Mag. A **67**, 1037 (1993).
[31]B. Kalisky, J. R. Kirtley, J. G. Analytis, J.-H. Chu, A. Vailionis, I. R. Fisher, and K. A. Moler, Phys. Rev. B **81**, 184513 (2010).
[32]H. Xiao, T. Hu, A. P. Dioguardi, N. Roberts-Warren, A. C. Shockley, J. Crocker, D. M. Nisson, Z. Viskadourakis, X. Tee, I. Radulov, C. C. Almasan, N. J. Curro, and C. Panagopoulos, Phys. Rev. B **85**, 024530 (2012).
[33]J. L. Niedziela, M. A. McGuire, and T. Egami, Phys. Rev. B **86**, 174113 (2012).
[34]M. J. Han, Q. Yin, W. E. Pickett, and S. Y. Savrasov, Phys. Rev. Lett. **102**, 107003 (2009).
[35]Q. Huang, Y. Qiu, W. Bao, M. A. Green, J. W. Lynn, Y. C. Gasparovic, T. Wu, G. Wu, and X. H. Chen, Phys. Rev. Lett. **101**, 257003 (2008).
[36]S. D. Wilson, Z. Yamani, C. R. Rotundu, B. Freelon, E. Bourret-Courchesne, and R. J. Birgeneau, Phys. Rev. B **79**, 184519 (2009).
[37]H. Gretarsson, A. Lupascu, J. Kim, D. Casa, T. Gog, W. Wu, S. R. Julian, Z. J. Xu, J. S. Wen, G. D. Gu, R. H. Yuan, Z. G. Chen, N.-L. Wang, S. Khim, K. H. Kim, M. Ishikado, I. Jarrige, S. Shamoto, J.-H. Chu, I. R. Fisher, and Y.-J. Kim, Phys. Rev. B **84**, 100509 (2011).
[38]P. Vilmercati, A. Fedorov, F. Bondino, F. Offi, G. Panaccione, P. Lacovig, L. Simonelli, M. A. McGuire, A. S. M. Sefat, D. Mandrus, B. C. Sales, T. Egami, W. Ku, and N. Mannella, Phys. Rev. B **85**, 220503 (2012).
[39]S.-H. Baek, N. J. Curro, T. Klimczuk, E. D. Bauer, F. Ronning, and J. D. Thompson, Phys. Rev. B **79**, 052504 (2009).
[40]J. Wu, P. Phillips, and A. H. Castro Neto, Phys. Rev. Lett. **101**, 126401 (2008).
[41]P. Hansmann, R. Arita, A. Toschi, S. Sakai, G. Sangiovanni, and K. Held, Phys. Rev. Lett. **104**, 197002 (2010).
[42]Z. P. Yin, K. Haule, and G. Kotliar, Nature Mater. **10**, 932 (2011).
[43]A. Georges, L. de' Medici, and J. Mravlje, Annu. Rev. Condens. Matter Phys. **4**, 137 (2013).
[44]T. Miyake, K. Nakamura, R. Arita, and M. Imada, J. Phys. Soc. Jpn. **79**, 044705 (2010).
[45]K. Haule and G. Kotliar, New J. Phys. **11**, 025021 (2009).
[46]K. Nakamura, R. Arita, and M. Imada, J. Phys. Soc. Jpn. **77**, 093711 (2008).
[47]V. Anisimov, E. Kurmaev, A. Moewes, and I. Izyumov, Physica C: Supercond. **469**, 442 (2009).
[48]P. Werner, M. Casula, T. Miyake, F. Aryasetiawan, A. J. Millis, and S. Biermann, Nat. Phys. **8**, 331 (2012).
[49]G. Kresse and J. Furthmüller, Phys. Rev. B **54**, 11169 (1996).
[50]G. Kresse and D. Joubert, Phys. Rev. B **59**, 1758 (1999).
[51]Z. P. Yin and W. E. Pickett, Phys. Rev. B **80**, 144522 (2009).
[52]T. Shimojima, K. Ishizaka, Y. Ishida, N. Katayama, K. Ohgushi, T. Kiss, M. Okawa, T. Togashi, X.-Y. Wang, C.-T. Chen, S. Watanabe, R. Kadota, T. Oguchi, A. Chainani, and S. Shin, Phys. Rev. Lett. **104**, 057002 (2010).